J. Vis. Commun. Image R. 66 (2020) 102732

Contents lists available at ScienceDirect

J. Vis. Commun. Image R.

journal homepage: www.elsevier.com/locate/jvci

A novel dark channel prior guided variational framework for underwater image restoration ☆

Guojia Hou *, Jingming Li, Guodong Wang, Huan Yang, Baoxiang Huang, Zhenkuan Pan *

College of Computer Science & Technology, Qingdao University, Qingdao 266071, PR China

ARTICLE INFO

Article history:
Received 16 July 2019
Revised 29 October 2019
Accepted 1 December 2019
Available online 14 December 2019

Keywords:
Underwater image restoration
Dehazing and denoising
UTV
ADMM
UDCP

ABSTRACT

Image captured underwater often suffers from low contrast, color distortion and noise problems, which is caused by absorbing and scattering before the light reaches the camera when traveling through water. Underwater image enhancement and restoration from a single image is known to be an ill-posed problem. To overcome these limitations, we establish an underwater total variation (UTV) model relying on underwater dark channel prior (UDCP), in which UDCP is used to estimate the transmission map. We design the data item and smooth item of the unified variational model based on the underwater image formation model. We further employ the alternating direction method of multipliers (ADMM) to accelerate the solving procedure. Numerical experiential results demonstrate that our underwater variational method obtains a good outcome on dehazing and denoising. Furthermore, compared with several other state-of-the-art algorithms, the proposed approach achieves better visual quality, which is illustrated by examples and statistics.

1. Introduction

On the account of an increasing number of underwater applications including oil and gas exploration, environmental and structural monitoring and inspections, object recognition and other related activities, underwater image processing has received considerable interest and attention among researchers. In the above-mentioned applications, the underwater environment is always observed by visual sensors, because the captured images or videos contain abundant information such as color, contour and texture that are easily identified and interpreted. Since the light scattering and color distortion vary with different wavelength in the underwater environment, this results in producing poor visibility images. Underwater captured images are usually degraded with low contrast, blurring or invisible, color distortion, non-uniform illumination and noise. Underwater images can hardly be used for further applicaitons without any pre-processing, such as underwater saliency detection [1,2], underwater object detection and recognition [3,4]. Therefore, it is essential to design effective methods for underwater image enhancement and restoration.

Many efforts have been devoted to restore and enhance degraded underwater images. Algorithms and techniques can be divided into two categories: one is based on image enhancement [5,6]. These approaches do not depend on any physical models, and are always committed to obtaining aesthetically pleasing images. For example, histogram equalization [7], color correction [8,9], multiple images-based methods [10] and fusion based methods [11,12]. Another kind of approaches is based on physical degradation model [13,14]. Wang et al. [15] proposed an effective method based on an underwater light propagation model. The forward scattering and non-uniform illumination are eliminated using blue-green dark channel prior. In [16], a novel signal underwater image restoration method based on non-local adaptive attenuation-curve prior was designed, in which the prior is used to estimate the transmission map (TM) relying on the distribution of pixel values on the curves. Recently, Zhang and Peng [17] designed a new underwater image formation mode for underwater image restoration, in which they took the properties of light into account and the TM was estimated based on joint prior.

The above methods all ignore the effect of noise, but in most cases, underwater image simultaneously suffers from low contrast, haziness, color reduction and noise. To resolve these problems, many researchers have adopted multi-stage methods to enhance and restore underwater image [18,19]. In [20], an automatic underwater image pre-processing method (including homomorphic

☆ This paper has been recommended for acceptance by Zicheng Liu.

* Corresponding authors at: College of Computer Science & Technology, Qingdao University, Qingdao 266071, PR China.
E-mail addresses: hgjouc@126.com (G. Hou), zkpan@126.com (Z. Pan).

https://doi.org/10.1016/j.jvcir.2019.102732
1047-3203/

filtering, wavelet denoising, anisotropic filtering, and contrast stretching) was presented to restore image visibility and eliminate underwater disturbance. Their contributions include inhomogeneous illumination correction, noise suppression, edge enhancement and color adjustment. Luan et al. [21] combined several algorithms for underwater image enhancement. The authors proved their effectiveness in improving contrast and suppressing noise combining homomorphic filtering algorithm, contrast stretching algorithm and wavelet domain denoising algorithm. Afterward, a novel method using a weighted guided trigonometric filter and an efficient automatic color enhancement algorithm are both introduced in [22]. Their contributions are global contrast improvement and noise suppression, and uneven color compensation. Pan et al. [23] proposed another two-stage underwater image de-scattering and enhancing method. They employed the convolutional neural network and adaptive bilateral filter to estimate and refine the TM. The recovered image was further transformed into the hybrid wavelets and directional filter banks domain to reduce noise and enhance edge. Unfortunately, due to the influence of multiple factors coupling, the traditional multi-stage method is often regarded as 'attend to one thing and lose another'.

In recent years, variational methods have been widely used in image processing. Lu et al. [24] introduced some state-of-the-art representative high-order variational models and further provided detailed discretization of these models. Afterward, Duan et al. [25] presented a nonlocal color multichannel model for color texture image inpainting. Wang et al. [26] designed three multichannel total variational models for image dehazing and denoising, and they further employed the split Bregman algorithm to improve computing efficiency. The foremost application of the variational model is the total variation (TV) model [27], which has a good performance in image denoising. It can also be said that the TV model provides a theoretical basis for variational image processing. Subsequently, the corresponding methods and technologies are further applied to other applications, such as image restoration [28–30], recognition [31,32], and segmentation [33–35]. In these literatures, the conventional split Bregman algorithm was mainly employed to accelerate the progress of the proposed models by authors.

The innovation of our approach is activated by the variational framework for Retinex. More variational models of Retinex for image enhancement and restoration are summarized in [36]. In 2003, Kimmel et al. [37] proposed a variational model of Retinex problem motivated by Retinex theory. The proposed formulation unified the previous different Retinex methods. Fang et al. [38] proposed a new fast variational approach to dehaze and denoise simultaneously, and the TM was estimated by using window adaptive method. Moreover, the multiple-splitting Chambolle-Pock algorithm without inner loop was used to boost its efficiency. Liang and Zhang [39] presented a convex variational model for the Retinex based on high-order total variation and L^1 decomposition. They speeded up the computational efficiency via primal–dual splitting method. Afterward, Ko et al. [40] minimized the L^2-norm data-fidelity and smoothness terms and split the L^1-derivative term according to the split Bregman iteration. In the same year, a new variational Retinex model with global sparse gradient guided was proposed by Zhang et al. [41]. Recently, Pu et al. [42] developed a fractional-order variation model for Retinx to enhance textural details and maintain contour features. In [43,44], Nnolim proposed an underwater image processing algorithm based on partial differential equation (PDE). A considerable of experimental analysis indicates that this method is superior to other algorithms in terms of contrast enhancement, color correction and noise suppression.

In this paper, inspired by PDE-based and variational Retinex method, we propose a novel approach based on underwater image formation model combining underwater dark channel prior (UDCP). The proposed method can achieve a good performance on dehazing, contrast enhancement, edge preservation, and noise suppression. The contributions of the paper are summarized as follows:

(i) A novel total variation method for underwater image restoration is proposed based on the underwater dark channel prior, in which we successfully integrate the underwater image formation model into the variational framework.
(ii) Rather than estimating the TM directly using the traditional dark channel prior, we present a UDCP method to improve the estimation of the TM. Moreover, we determine the global background light from the candidate pixels estimated from the brightest regions.
(iii) In order to reduce the complexity of solving the proposed underwater total variation (UTV) model, we design a fast algorithm based on the alternating direction method of multipliers (ADMM) to accelerate the whole progress.
(iv) Compared with previous methods, the proposed underwater variational method can achieve a good performance on dehazing, denoising, and improving contrast simultaneously.

The rest of our work is organized as follows. Section 2 briefly introduces background information and related algorithms. Then, the proposed method is presented in Section 3. Section 4 shows the experimental results and discussion. Finally, the conclusions and future work are provided in Section 5.

2. Background and related work

The first underwater imaging model was proposed by McGlamery [45], Jaffe [46] and is applied to the development of various underwater image acquisition systems, namely Jaff-McGlamery model.

Given that I is the observed degradation color image, J is the non-degraded image, the fogging model to represent the degradation of a haze image can be defined as follows.

$$\mathrm{I}^c(x) = J^c(x) \cdot t(x) + A^c(1 - t(x)), \tag{1}$$

where A is the air light, t is the medium transmission along the scene, and c is a color channel, $c \in \{r, g, b\}$.

To some degree, the process of underwater degradation produced is similar to the fogging model, this model can also be used for underwater image restoration. In [47], the underwater optical model is mathematically defined as

$$\mathrm{I}^c(x) = \mathrm{J}^c(x) \cdot t(x) + \mathrm{B}^c(1 - t(x)), \tag{2}$$

where B is global background light, I, J, t and c denote the same represents as given in (1).

Since only the observed degraded underwater image I is given, we need to estimate t, B, and recover J from I. To estimate B and t, dark channel prior (DCP) method [48] is widely used because the fog scene is similar to the underwater environment. Unfortunately, a direct application of DCP method for underwater image enhancement and restoration resulting in displaying low brightness and reducing visibility, and obscuring many details. Another effective enhancement approach is introduced in [49], they deduced a new underwater optical model for the underwater image to improve their perception. The scattering rate and the transmission are estimated based on UDCP. The UDCP which is redefined according to He et al.'s DCP theory. As the energy of red light being absorbed largely, they only consider the green and blue channels

in the underwater dark channel. The UDCP for a degrade underwater image is described as

$$J^{uwdark}(x) = \min_{c' \in \{g,b\}} \left(\min_{y \in \Omega(x)} \left(J^{c'}(y) \right) \right), \tag{3}$$

where J^{uwdark} represents the image in underwater dark channel, the $y \in \Omega(x)$ is a square local patch centered at x, $c' \in \{g, b\}$. Empirically, in most cases, the intensity value of the underwater dark channel is also approximately zero.

Assuming the transmission of the green and blue color channels are identical, one can further take the min operation on the two color channels in the local patch. The estimated transmission map $\tilde{t}$ in each patch can be defined as:

$$\min_{y \in \Omega(x)} \left(\min_{c'} \left(\frac{I^{c'}(y)}{B^{c'}} \right) \right) = \tilde{t}(x) \min_{y \in \Omega(x)} \left(\min_{c'} \left(\frac{J^{c'}(y)}{B^{c'}} \right) \right) + 1 - \tilde{t}(x), \tag{4}$$

The UDCP denotes that $J^{undark}(x) \to 0$, which indicates that

$$\min_{y \in \Omega(x)} \left(\min_{c'} \frac{J^{c'}(y)}{B^{c'}} \right) = 0. \tag{5}$$

Then, the estimated TM in (4) can be obtained as

$$\tilde{t}(x) = 1 - \min_{y \in \Omega(x)} \left(\min_{c'} \frac{I^{c'}(y)}{B^{c'}} \right). \tag{6}$$

The patch size is empirically selected between 11×11 and 51×51. In most scenarios, the existence of haze makes people feel the depth of field, so it is necessary to keep a certain amount of haze in the underwater image. This can be achieved by introducing a factor ω between [0, 1] in (6), its value is application-based, then (6) is modified as

$$\tilde{t}(x) = 1 - \omega \min_{y \in \Omega(x)} \left(\min_{c'} \frac{I^{c'}(y)}{B^{c'}} \right). \tag{7}$$

The background light (BL) B^c is usually empirically picked with the brightest pixel in an image, which is estimated as

$$B^{c'} = \max_{x \in I} \min_{y \in \Omega(x)} \left(\min_{c'} I^{c'}(y) \right) = 0. \tag{8}$$

However, in some cases, this assumption is too simple to be robust to the erroneous. Instead of selecting the highest pixel, He et al. chosed the top 0.1% pixel as the value of B. However, this method is often inaccurate when applied in the underwater scene, and it is easy to mistake the bright point in the foreground as the background light, resulting in an unsatisfactory recovered image. To overcome this drawback, a method for wavelength compensation and image dehazing (WCID) [50] was proposed to restore underwater images. Wherein the foreground and the background can be segmented once the depth map is estimated. The WCID method could successfully remove the haze and balance color, but failed to suppress noise. Afterward, Li et al. [51] proposed an underwater dehazing algorithm with minimum information loss and a contrast enhancement algorithm with histogram distribution prior. They employed a hierarchical searching method derive from quad-tree subdivision to robustly estimate the BL. Furthermore, they used a red channel prior to estimate the TM. But in fact, the energy of red light is absorbed largely around deep-water area. Consequently, the red channel cannot provide enough information of depth map. Besides, most aforementioned methods may achieve some unpleasant results especially in the challenging underwater scenes (i.e., heavy haze scene or turbid scene). We handle this issue with the help of the so-called UDCP method as previously described.

3. The proposed method

In this section, we first establish a novel UDCP Guided total variation model and then design an alternating direction multiplier method to solve the energy equation of our variational framework. Fig. 1 presents a general flowchart of the proposed method.

3.1. Underwater total variation model

As mentioned above, taking the noise into consideration, the underwater imaging model can be expressed as

$$I_c = J_c \cdot t + (1 - t) \cdot B_c + n, \tag{9}$$

where I, J, B, t and c represent the same definitions, which is denoted in (1), and n is the noise. Obviously, (9) can be rearranged as

$$B_c - I_c + n = (B_c - J_c) \cdot t. \tag{10}$$

To simplify the product form, one can convert (10) into the logarithmic domain

$$f = u + t', \tag{11}$$

where $f = \log(B_c - I_c + n)$, $u = \log(B_c - J_c)$, $t' = \log t$.

According to Tikhonov model and Kimmel's variational Retinex algorithm, the minimization of following energy functional is proposed to recover the haze-free and noise-free underwater image simultaneously:

$$\min_{u,t'} E(u, t') = \left\{ \begin{array}{c} \lambda \int_\Omega |\nabla u| dxdy + \mu \int_\Omega |\nabla t'| dxdy \\ + \frac{1}{2} \int_\Omega (u - f + t')^2 dxdy \end{array} \right\}, \tag{12}$$

where λ and μ are free non-negative real parameters which determine the degree of denoising and dehazing, and the larger values indicate more important on the corresponding items. In (12), the first two terms are the smoothness times, and the last one is the data fidelity item.

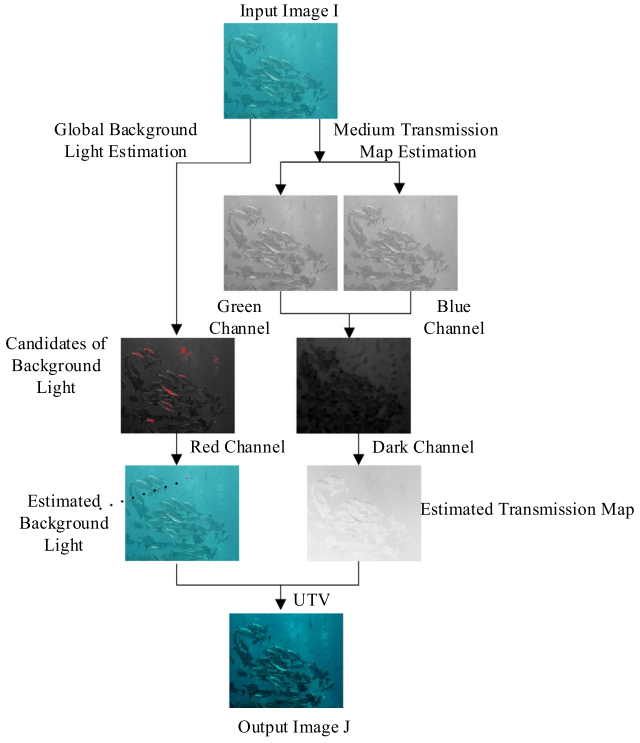

Fig. 1. The general flowchart of the proposed method.

In our framework, the initial value t_0 of t can be obtained using the underwater dark channel prior mentioned in Section 2. Due to the background of an underwater scene tends to be green or blue, the method to estimated background ground B by picking the top 0.1% in the dark channel is ill-suited for underwater image. Here, we select the top 1% brightest pixels in the red channel, and then pick the 'brighter pixel' in the above-elected pixels as the value of the BL. Wherein, the selection of the 'brighter pixel' points is to arrange the red channel intensity values of the 1% brightest pixel points from low to high, and then take the pixels in the first quarter as the 'brighter pixel'.

3.2. ADMM algorithm for UTV

The problem of (12) is mathematically an ill-posed problem, which can be directly solved by a fast-computational algorithm based on the alternating direction method of multipliers [52]. Its implementation for UTV model is given below.

After adding $\vec{w} = (w_1, w_2)^T = \nabla u$ and $\vec{v} = (v_1, v_2)^T = \nabla t'$ that are two auxiliary vector variables, we can transform (12) into

$$\begin{aligned}&\left(u, t', \vec{w}, \vec{v}\right)\\ &= \underset{u,t',\vec{w},\vec{v}}{\operatorname{argmin}} \left\{ \begin{array}{c} \lambda \int_\Omega |\vec{w}| dxdy + \mu \int_\Omega |\vec{v}| dxdy + \frac{1}{2}\int_\Omega (f-u-t')^2 dxdy \\ + \int_\Omega \vec{\alpha}\left(\vec{w}-\nabla u\right)dxdy + \int_\Omega \vec{\beta}\left(\vec{v}-\nabla t'\right)dxdy \\ + \frac{\theta_1}{2}\int_\Omega |\vec{w}-\nabla u|^2 dxdy + \frac{\theta_2}{2}|\vec{v}-\nabla t'|^2 dxdy \end{array} \right\} \\ &\qquad s.t.\ \ t \in (0,1)\end{aligned} \tag{13}$$

where $\vec{\alpha}$ and $\vec{\beta}$ represent the Lagrange multipliers, their values are often simply initialized to zero. θ_1 and θ_2 are penalty parameters which are used to compensate for the Lagrange items. ∇ represents gradient. Both the Lagrange multipliers item and penalty parameter item are introduced to ensure that $\vec{w}$ is closer to ∇u and $\vec{v}$ is closer to $\nabla t'$.

After using the alternating iterative optimization of variables, the solution of (13) can be decomposed into four subproblems:

$$\varepsilon_1(u) = \min_u \left\{ \begin{array}{c} E(u) = \frac{1}{2}\int_\Omega (f-u-t')^2 dxdy \\ + \int_\Omega \vec{\alpha}\left(\vec{w}-\nabla u\right)dxdy + \frac{\theta_1}{2}\int_\Omega |\vec{w}-\nabla u|^2 dxdy \end{array} \right\}, \tag{14a}$$

$$\varepsilon_2(t') = \min_{t'} \left\{ \begin{array}{c} E(t') = \frac{1}{2}\int_\Omega (f-u-t')^2 dxdy \\ + \int_\Omega \vec{\beta}\left(\vec{v}-\nabla t'\right)dxdy + \frac{\theta_2}{2}|\vec{v}-\nabla t'|^2 dxdy \end{array} \right\}, \tag{14b}$$

$$\varepsilon_3\left(\vec{w}\right) = \min_{\vec{w}} \left\{ \begin{array}{c} E\left(\vec{w}\right) = \lambda \int_\Omega |\vec{w}| dxdy \\ + \int_\Omega \vec{\alpha}\left(\vec{w}-\nabla u\right)dxdy + \frac{\theta_1}{2}\int_\Omega |\vec{w}-\nabla u|^2 dxdy \end{array} \right\}, \tag{14c}$$

$$\varepsilon_4\left(\vec{v}\right) = \min_{\vec{w}} \left\{ \begin{array}{c} E\left(\vec{v}\right) = \mu \int_\Omega |\vec{v}| dxdy \\ + \int_\Omega \vec{\beta}\left(\vec{v}-\nabla t'\right)dxdy + \frac{\theta_2}{2}\int_\Omega |\vec{v}-\nabla t'|^2 dxdy \end{array} \right\}, \tag{14d}$$

Then the process of the iterative solution can be decomposed into the following five sub-procedure.

Sub 1: Fix $t'^k, \vec{w}^k, \vec{v}^k$ to calculate u^{k+1}.

The Euler-Lagrange equation of (14a) is

$$\left\{ \begin{array}{ll} u - f + t' + \nabla\vec{\alpha}^k + \theta_1 \nabla w^k - \theta_1 \Delta u^{k+1} = 0 & in\ \Omega \\ \vec{\alpha}\cdot\vec{n} + \theta_1\left(\nabla u^{k+1} - \vec{w}^k\right)\cdot\vec{n} = 0 & on\ \partial\Omega \end{array} \right. . \tag{15}$$

where $\vec{n}$ is normal vector, Δ represents divergence.

After using the Gauss–Seidel iteration method, (15) can be discretized as

$$u_{ij}^{k+1} = \frac{f - t' - \nabla\vec{\alpha}^k - \theta_1 \nabla\vec{w}^k - \frac{\theta_1}{h^2}\left(u_{i-1,j}^{k+1} + u_{i+1,j}^k + u_{ij-1}^{k+1} + u_{ij+1}^k\right)}{1 + \frac{4\theta_1}{h^2}} \tag{16}$$

where k is the number of iterations steps, h is the iteration step-size, i and j are the coordinates of image pixel.

Sub 2: Fix $u^{k+1}, \vec{w}^k, \vec{v}^k$ to calculate t'^{k+1}.

The Euler-Lagrange equation of (14b) is

$$\left\{ \begin{array}{ll} u - f + t' + \nabla\vec{\beta} + \theta_2 \nabla\vec{v} - \theta_2 \Delta t' = 0 & in\ \Omega \\ \vec{\beta}\cdot\vec{n} + \theta_2\left(\nabla t - \vec{v}\right)\cdot\vec{n} = 0 & on\ \partial\Omega \end{array} \right. , \tag{17}$$

the solution of t'^{k+1} in (17) can be similarly analytical obtained

$$t_{i,j}'^{k+1} = \frac{f - u - \nabla\vec{\beta}^k - \theta_2 \nabla\vec{v}^k - \frac{\theta_2}{h^2}\left(t_{i-1,j}'^{k+1} + t_{i+1,j}'^k + t_{ij-1}'^{k+1} + t_{ij+1}'^k\right)}{1 + \frac{4\theta_2}{h^2}}. \tag{18}$$

Sub 3: Fix $u^{k+1}, t'^{k+1}, \vec{v}^k$ to calculate $\vec{w}^{k+1}$.

The Euler-Lagrange equation of (14c) is

$$\frac{\lambda}{\theta_1}\cdot\frac{\vec{w}^{k+1}}{\left|\vec{w}^{k+1}\right|} + \vec{w}^{k+1} - \left(\nabla u^{k+1} - \frac{\vec{\alpha}^k}{\theta_1}\right), \tag{19}$$

the solution of $\vec{w}^{k+1}$ in (19) can be solved using generalized soft threshold formulation (GSTF) that is

$$\vec{w}^{k+1} = \max\left(\left|\nabla u^{k+1} - \frac{\vec{\alpha}^k}{\theta_1}\right| - \frac{\lambda}{\theta_1}, 0\right)\cdot\frac{\nabla u^{k+1} - \frac{\vec{\alpha}^k}{\theta_1}}{\left|\nabla u^{k+1} - \frac{\vec{\alpha}^k}{\theta_1}\right|}. \tag{20}$$

Sub 4: Fix $u^{k+1}, t'^{k+1}, \vec{w}^{k+1}$ to calculate $\vec{v}^{k+1}$.

The Euler-Lagrange equation of (14d) is

$$\frac{\mu}{\theta_2}\cdot\frac{\vec{v}^{k+1}}{\left|\vec{v}^{k+1}\right|} + \vec{v}^{k+1} - \left(\nabla t'^{k+1} - \frac{\vec{\beta}^k}{\theta_2}\right), \tag{21}$$

and its corresponding GSTF is

$$\vec{v}^{k+1} = \max\left(\left|\nabla t'^{k+1} - \frac{\vec{\beta}^k}{\theta_2}\right| - \frac{\mu}{\theta_2}, 0\right)\cdot\frac{\nabla t'^{k+1} - \frac{\vec{\beta}^k}{\theta_2}}{\left|\nabla t'^{k+1} - \frac{\vec{\beta}^k}{\theta_2}\right|}. \tag{22}$$

Sub 5: Update the Lagrange multipliers $\vec{\alpha}$ and $\vec{\beta}$ in (13)

$$\left\{ \begin{array}{l} \vec{\alpha}^{k+1} = \vec{\alpha}^k + \theta_1\left(\vec{w}^{k+1} - \nabla u^{k+1}\right) \\ \vec{\beta}^{k+1} = \vec{\beta}^k + \theta_2\left(\vec{v}^{k+1} - \nabla t'^{k+1}\right) \end{array} \right. \tag{23}$$

4. Experimental results and discussion

In this section, the performance of the proposed method, qualitative comparison and quantitative comparison are carried out, respectively. Several underwater images suffer from low contrast,

fog, and noise are considered for testing and comparing applications. All experiments are performed using Matlab 2016b on a Windows 10 PC with an Intel(R) Core(TM) i7-8500U at 3.2 GHz and 8 GB RAM. In what follows, we set the parameters of (13) to $\lambda = 0.01$, $\mu = 10$, $\theta_1 = 0.001$, $\theta_2 = 0.3$, and initialize $\vec{\alpha}$ and $\vec{\beta}$ to $\vec{0}$. Moreover, we employ the stopping criteria algorithm $\left|E^{k+1} - E^k\right|/E^k \leqslant \varepsilon$ to keep the convergence of the proposed model, where E is energy function and ε ($\varepsilon = 10^{-4}$) is an extremely small number to terminate the iteration.

4.1. Performance of proposed method

In this part, we conduct a series of experiments to demonstrate the performance, robustness and effectiveness of the proposed method. Firstly, three representative underwater images with different conditions are tested to evaluate its' performance, as shown in Fig. 2. From Fig. 2(a), we can see that the original underwater images show hazy, low light or noise. It can also be observed from their corresponding dark channel in Fig. 2(b) that there are some bright pixels in foggy regions. However, the recovered images in Fig. 2(c) present that our method can effectively improve visibility and brightness, and uncovering more details. As observing from the dark channel in Fig. 2(d) obtained from restored images, we can see that the original white area of Fig. 2(b) becomes darker, which proves that our UTV has a good performance on removing haze.

Furthermore, the histogram distribution of R, G and B channels of three original underwater images of Fig. 2(a) presented in Fig. 3 (a) and the corresponding results after using our method are orderly displayed in Fig. 3(b). As shown in the left side of each set of Fig. 3(a), they all concentrate in one region (*e.g.*, the right two histograms of Fig. 3(a) concentrate in the left and intermediate sides, respectively) due to light absorption, light reflection, bending and scattering of light. From the right side of each set of Fig. 3b, we can observe that the histogram distribution after employing our approach prove to be wider and more consistent than those without post-processing. Additionally, combing with Fig. 2(c) and (d), we can conclude that the enhanced results obtain higher contrast and genuine color, and reveal clearer details.

As described previously, inaccurate TM or BL estimation often leads to an unsatisfying restoration result. In order to further analyze the effects of TM and BL estimation on the proposed method, several examples with different estimated values of TM and BL are illustrated Figs. 4 and 5. Fig. 4 presents two examples in which changing values of BL leads to different visual results. As shown in Fig. 4(b), the restoration results with bright BL estimation would generate dark scene radiance while using dim BL brings an opposite result. In contrast, observing from Fig. 4(c), we can see that using our BL estimated method described in Section 3.1 produces a more visually satisfying result. From the estimated transmission map of Fig. 5(b) and (c), we can observe that with properly estimated TM, the proposed can well remove the density of haze.

4.2. Qualitative comparison

In this visual comparison, the proposed approach is compared with six other techniques including histogram equalization (HE) method, multi-scale Retinex (MSR) method, dark channel prior (DCP) method, wavelength compensation and image dehazing (WCID) method, Li's dehazing and contrast enhancement method, and Ng's variational Retinex method [53]. Among these algorithms, HE and MSR methods are the two traditional methods for common image enhancement. Moreover, DCP, WCID and Li's algorithm are the state-of-the-art dehazing methods which employ the same underwater image formation model as well as our method. Additional, as the proposed method is designed using a variational framework, Ng's total variational model for Retinex is also included.

The visually compared results of different methods are illustrated in Fig. 6. Seven representative underwater color images with different degradations (i.e. fuzzy, hazy, color fading, artificial light, low-visibility, noise, and deep water scene) are selected for comparison as shown in Fig. 6(a). HE algorithm is essentially a nonlinear stretching and redistribution of image pixel values, which performs contrast stretching on the histogram distributed in the middle is enhanced. Fig. 6(b) shows that the HE algorithm can adjust contrast and enhance brightness, leading to an improvement for color correction and the visibility of details for underwater images, but it contains over-enhanced regions and amplifies noise. In Fig. 6(c), for all of the challenging scenes, MSR method presents unsatisfactory results because it is specially designed for ground-truth images and doesn't take the light absorption and scattering into consideration. Besides, due to the limitations of the algorithm itself, the common shortcomings of MSR are partial color distortion, unclear texture, no noticeable improvement in highlight areas. Additionally, both the HR and MSR algorithms are compared to state that the traditional enhancement methods are not suitable for underwater image.

On account of basing on the same image dehazing model, DCP, WCID and Li's methods all generate good results on removing the haze, as shown in Fig. 6(d)–(f). DCP method estimates the TM based on dark channel prior but still failing to recover the image

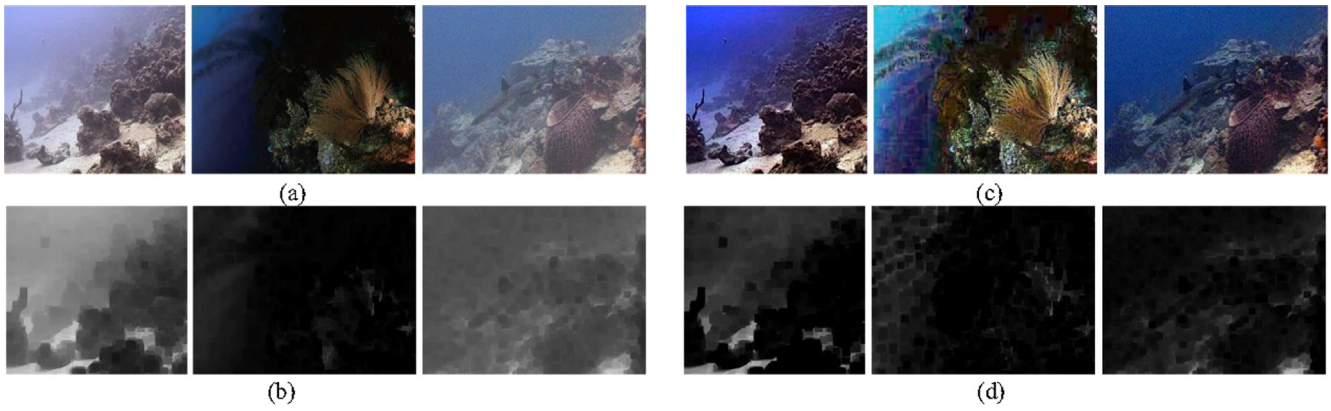

Fig. 2. Real underwater images test: (a) three original underwater images; (b) the dark channel obtained form (a); (c) the restored results generated by the proposed method; (d) the dark channel obtained from (c).

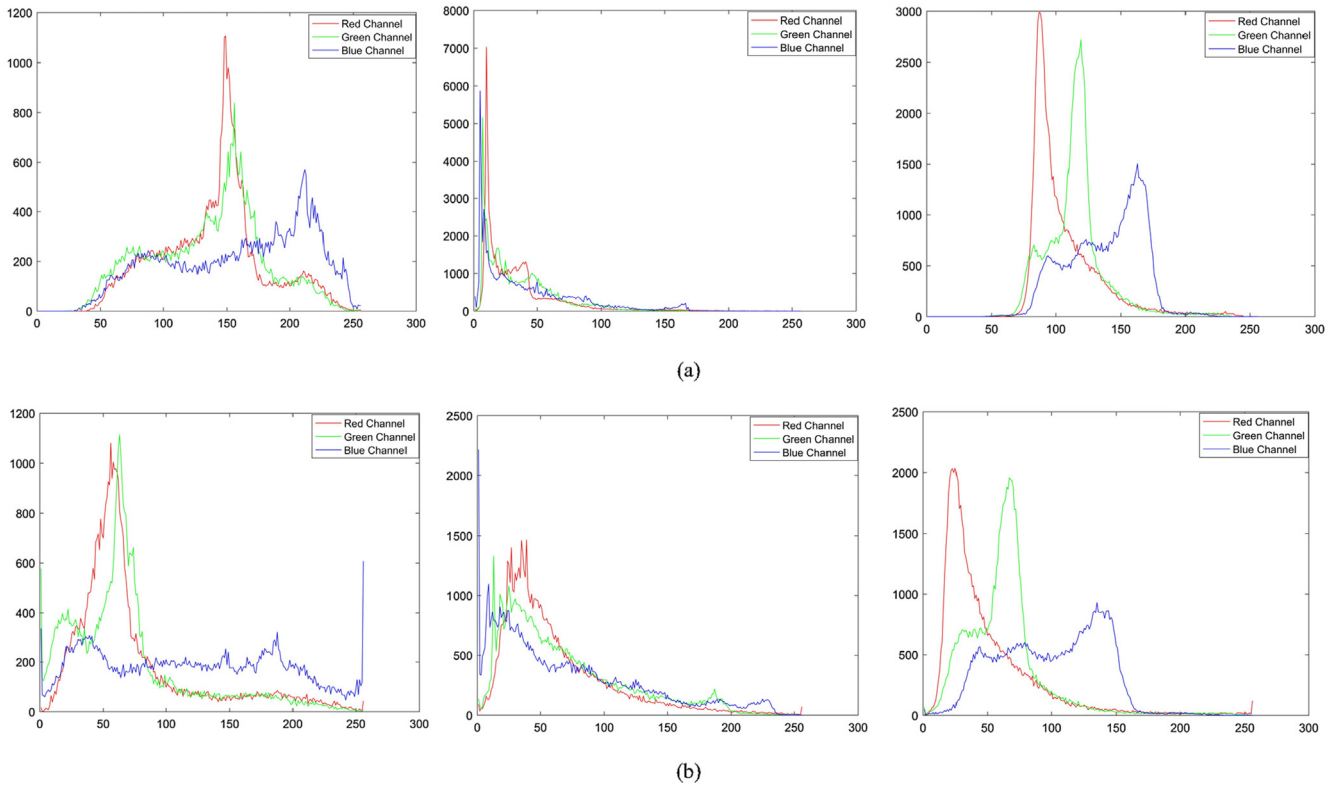

Fig. 3. Histogram distribution of R, G, and B channels. (a) Histogram distributions of R, G, and B channels of the three original underwater images in Fig. 2(a); (b) the corresponding Histogram distributions of R, G, and B channels after employing proposed method. In the histogram distributions, the x-axis represents the gray levels, the y-axis represents the normalized frequency.

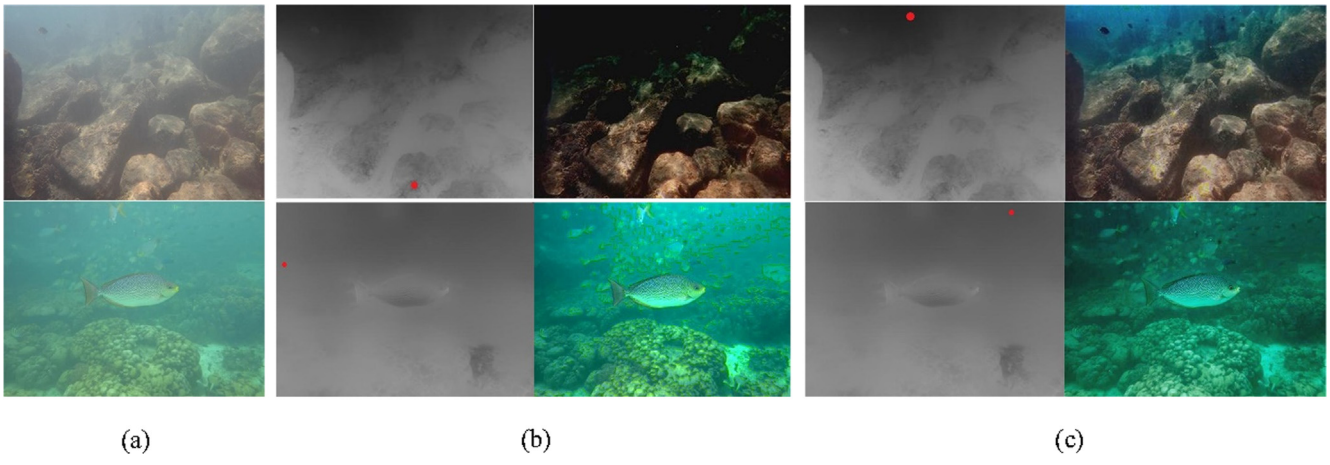

Fig. 4. Examples of inaccurate and accurate BL estimation. (a) Original underwater images, (b) restored results with bright BL (marked with a red dot in the top row) and dim BL (marked with a red dot in the bottom row), (c) the corresponding restored results with BL estimation from the algorithm described in Section 3.1. (For interpretation of the references to color in this figure legend, the reader is referred to the web version of this article.)

for which BL simply replaced with the brightest pixel is inaccurate in the underwear scene. Besides, for the underwater image taken under the fuzzy scene, DCP method has little effect on the results, because it is seriously degraded by color faded and low visibility, as shown in Fig. 6(d). In Fig. 6(e), we can see that the WCID method achieves a better performance than HE and MSR algorithms, which can solve the overflow problem of highlight parts in the image and avoid excessively magnified noise. But it still cannot achieve a visually satisfactory outcome. Like DCP algorithm, it erroneously estimates the underwater TM in R, G, B channels and incorrectly considers some foreground pixels as background light. In these examples, owing to the overestimation of the thickness of the haze and inaccurate estimation of BL, DCP and WCID algorithm generate dark images with color distortion. In Li's approach, different from DCP and WCID algorithms, the underwater BL is estimated based on hierarchical searching technology and the medium transmission map is estimated mainly depending on the degraded channel. Moreover, the combination of dehazing algorithm and contrast enhancement algorithm are employed to increase contrast and brightness, visually, Li's method outperforms previous compared schemes as shown in Fig. 6(f). However, some regions are overexposed (*e.g.* the bright background regions) and lose many image

Fig. 5. An examples of inaccurate and accurate TM estimation. (a) Original underwater image, (b) the transmission map and restored result with inaccurate TM estimation, (c) the transmission map and restored result with TM estimation from the algorithm described in Section 3.1.

details (*e.g.* the corner of the image). Besides, the unsatisfactory results also come from without taking noise into the image dehazing model.

The obtained results of Fig. 6(g) show that the Ng's method can improve the brightness of the raw underwater images. However, because of without deriving from image dehazing model, it does not help remove the fog spray. And visually, similar to MSR algorithm, Ng's method assumes spatial smoothness of the illumination. It can be seen that the recovered results from both the methods aggravate the atomization effect because of erroneously estimated illumination image. As shown in Fig. 6(h), the proposed UTV method estimates TM and BL more precisely and successfully reappear visibility, eliminate non-uniform illumination, preserve color homogeneity, and reduce noise, better than the results of those outdoor image enhanced and restored methods and the results from state-of-the-art approaches designed for underwater images.

To further see the detailed superiority of the proposed method, we crop a red rectangle area from restored images after using several compared underwater restoration methods including WCID method, automatic red-channel (ARC) [54] method, Li's method, and Dehazenet [23] method, as shown in the first and third rows of Fig. 7. The corresponding zoomed small sub-regions are displayed in the second and fourth rows of Fig. 7. From Fig. 7, one can observe that the four compared method have similar problems in correcting color and eliminating non-uniform illumination. In contrast, after using our UTV method, the details information in rocks are well preserved, and the box in the images are enhanced moderately.

4.3. Quantitative comparison

In the following experiment, we compare the proposed approach with aforementioned methods using several no-reference metrics to conduct a quantitative analysis relying on some statistical values of the tested images. Here, four evaluation indicators [55,56] namely the rate of visible edges e, the saturation σ, the contrast restoration $\bar{r}$, and the underwater color image quality evaluation metric (UCIQE) Q [57] are employed for quantitative comparison. The value of e can be positive or negative. If it is negative, it means that the number of visible edges of the restored image decreases while the positive value means that it increases. The values of σ, $\bar{r}$ and Q are positive, in which σ and Q range from 0 to1, while the obtained $\bar{r}$ can be great than 1. For the e, $\bar{r}$ and Q, higher value shows better result; in contrast, for the σ, lower shows better result.

The e indicator is used to assess the ability to recover edges that were not visible in the original image I_o but are in the contrast restored image I_r. The $\bar{r}$ indicator represents the restored quality of contrast after employing the underwater restored method. Opposite to e, $\bar{r}$ indicator considers both visible and invisible edges in I_o. The σ indicator is denoted by calculating the number n_s of pixels which represent saturated. Their values are respectively defined as

$$\begin{cases} e = \frac{n_r - n_o}{n_o} \\ \bar{r} = \exp\left[\frac{1}{n_r}\sum_{P_i \in \wp_r} \log r_i\right] \quad with \;\; r = VL_r/VL_o \\ \sigma = \frac{n_s}{M \times N} \end{cases} \tag{27}$$

where, n_o and n_r are respectively the numbers of visible edges in I_o and I_r, and $\wp_r$ is the latter set. VL_r and VL_o are respectively the visibility level in I_o and I_r. $M \times N$ is the size of the image.

The metric Q is designed to evaluate the quality of restoration underwater image, which indicates the statistical distribution of the chroma, saturation, and contrast. Let $I_p = [l_p, a_p, b_p]$ be the pixel values for image I in CIELab space, $p = 1 \cdots N$. The image I has N pixels. Then, the definition of Q for I in CIELab space is given as

$$Q = c_1 \times \sigma_C + c_2 \times con_L + c_3 \times \mu_S, \tag{28}$$

where c_1, c_2, c_3 denote weighted coefficients selected as $c_1 = 0.468$, $c_2 = 0.2745$, $c_3 = 0.2576$.σ_C denotes the standard deviation of chroma, con_L denotes the contrast of luminance and μ_S denotes the average of saturation. Their corresponding formulas are

$$\begin{cases} \sigma_C = \sqrt{\frac{1}{N}\sum_{p=1}^{N}\left(C_p{}^2 + \mu_C{}^2\right)} \\ con_L = tol\_high - tol\_low \\ \mu_s = \sqrt{\frac{1}{N}\sum_{p=1}^{N}\frac{C_p}{L_p}} \end{cases} \tag{29}$$

where $C_p = \sqrt{a^2 + b^2}$, $\mu_C = \frac{1}{N}\sum_{p=1}^{N} C_p$, $tol\_high = 0.99$, $tol\_low = 0.01$.

To assess the effectiveness and robustness of the proposed method, we further compare the results of different methods on Fig. 6, as shown in Tables 1A and 1B. In these Tables, bold values express the best average results. In some scenarios, the higher scores in term of e, σ, $\bar{r}$, Q mean that our method for restoring underwater images achieves superior performance on color rendition, edge and texture preservation and nonuniform illumination elimination. As can be observed in Tables 1A and 1B, the values of e obtained from HE, DCP and WCID and Ng's methods are negative (−0.11, −0.27, −0.20, and −0.08, respectively) in deep water scenes, which indicate that they may cover some edges and details. Unfortunately, all values obtained by Ng's algorithm are less than 0.3. In contrast, the values of ours' are positive under all challenging scenes. Besides, the average value of the rate of visible edges is the highest at 0.554, which is at least 10% higher than the others'. The best e values indicate that our dehazing and denoising method outperforms the other six compared methods. For σ, WCID method achieves the best results owing to wavelength compensation. Their values for challenging underwater scenes are all zero. Unfortu-

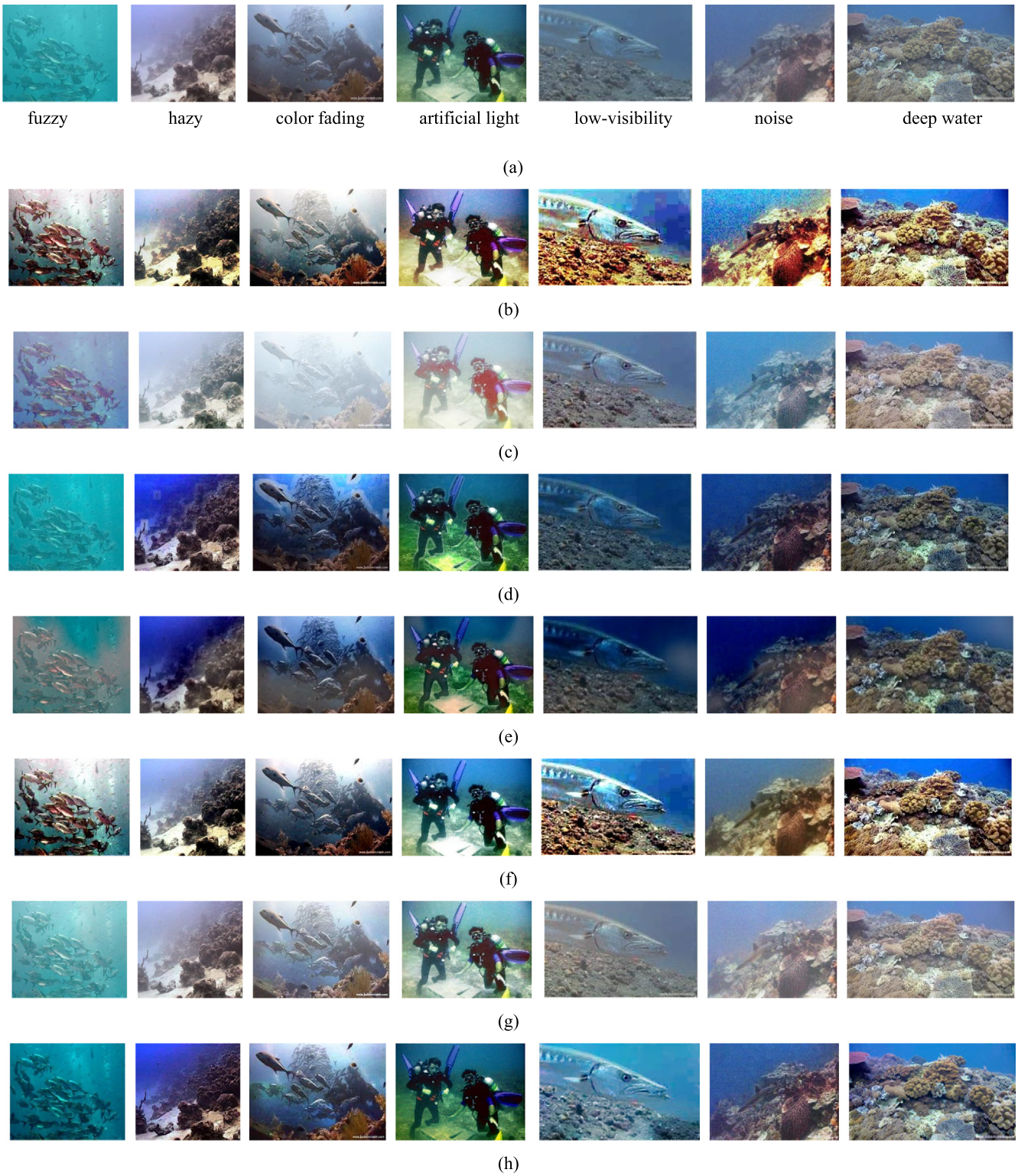

Fig. 6. Comparison on challenging underwater scenes. (a) Underwater images captured under challenging scenes. (b)–(h) Restored results after using HE, MSR, DCP [48], WCID [50], Li's [51], Ng's [53] and proposed method, respectively.

nately, combining with the qualitative measures, it shows that Li's and our algorithms give better visual results in color variation and brightness. For $\bar{r}$ and Q, our method still stands out excepting HE and Li's methods. However, for some images in Fig. 6(b) and (g), HE method results in noise amplification and color distortion. Similarly, Li's method tends to over enhance the local nonuniform illumination of the image. As we mentioned above, the metric Q is a linear combination of chroma, saturation, and contrast, and the indicator $\bar{r}$ is also used to assess the contrast. HE algorithm can obtain the highest value of $\bar{r}$(3.164) and Q (0.659) mainly due to

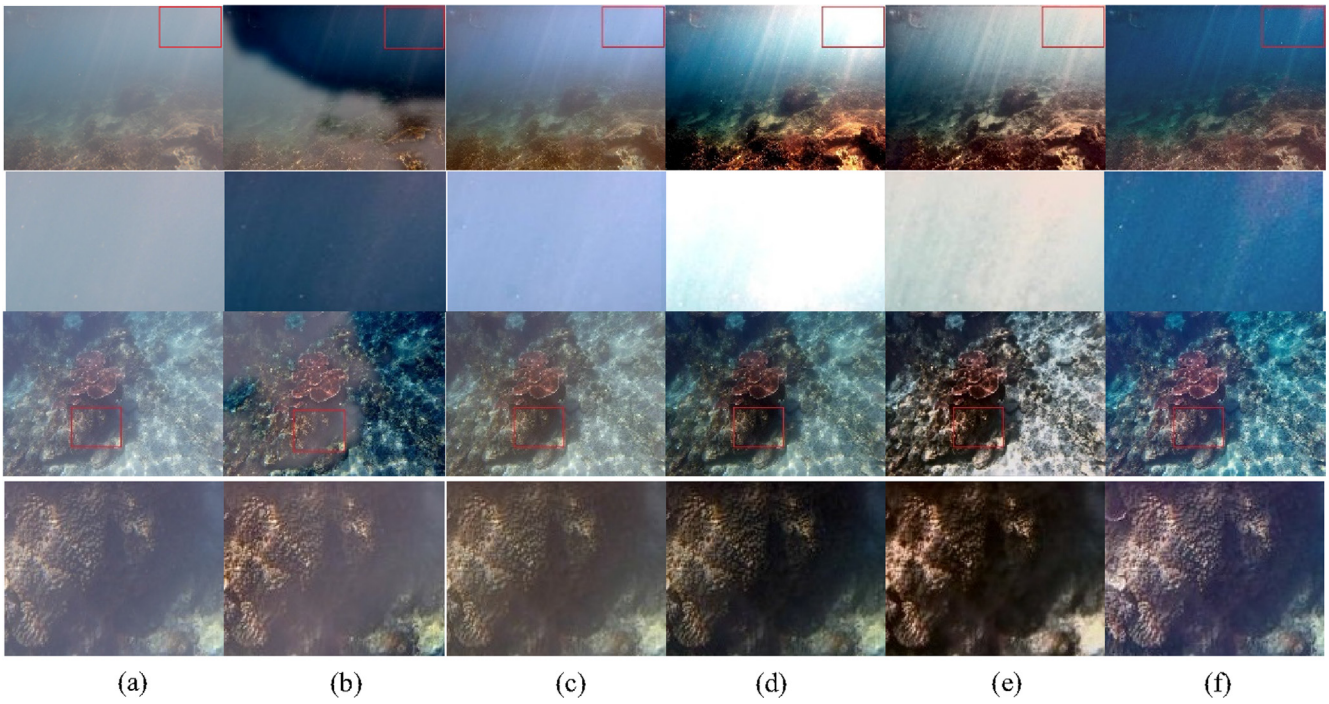

Fig. 7. Zoomed small sub-regions (marked in red rectangle) for detail comparison. (a) Original underwater image, (b–f) the corresponding restored results using WCID [50], ARC [54], Li's [51], Dehazenet [23] and the proposed method, respectively. (For interpretation of the references to color in this figure legend, the reader is referred to the web version of this article.)

Table 1A
Quantitative comparison of underwater restored images shown in Fig. 6 using seven compared methods. (The bold values express the best metric values).

Scenes	HE				MSR				DCP [48]				WCID [50]			
————	e	σ	$\bar{r}$	Q	e	σ	$\bar{r}$	Q	e	σ	$\bar{r}$	Q	e	σ	$\bar{r}$	Q
fuzzy	1.134	0.072	3.728	0.618	0.349	0.000	1.455	0.422	0.247	0.000	1.115	0.353	0.414	0.001	3.871	0.439
hazy	0.237	0.178	1.690	0.612	−0.12	0.002	1.081	0.462	0.564	0.028	1.928	0.598	0.403	0.000	1.919	0.600
color fading	0.138	0.806	2.079	0.606	−0.77	0.000	0.717	0.332	0.323	0.000	1.843	0.615	0.108	0.000	2.581	0.596
artificial light	0.467	0.267	2.020	0.651	−0.66	0.064	1.182	0.448	0.937	0.032	1.526	0.651	0.742	0.000	2.265	0.626
low-visibility	0.290	0.007	4.997	0.712	−0.02	0.004	1.526	0.523	0.159	0.000	1.558	0.548	0.245	0.000	1.512	0.486
noise	0.715	0.430	4.672	0.727	0.156	0.001	1.509	0.514	0.654	0.000	1.633	0.594	0.870	0.000	1.413	0.567
deep water	−0.11	0.067	2.962	0.685	0.147	0.000	1.395	0.546	−0.27	0.022	1.571	0.581	−0.20	0.000	2.429	0.585
Average	0.410	0.261	**3.164**	**0.659**	−0.13	0.010	1.266	0.464	0.373	0.012	1.596	0.563	0.369	**0.000**	2.284	0.557

Table 1B
Quantitative comparison of underwater restored images shown in Fig. 6 using seven compared methods. (The bold values express the best metric values).

Underwater scenes	Li [51]				Ng [53]				Proposed			
————	e	σ	$\bar{r}$	Q	e	σ	$\bar{r}$	Q	e	σ	$\bar{r}$	Q
fuzzy	1.151	0.969	3.729	0.622	0.203	0.000	1.372	0.374	0.698	0.000	1.312	0.584
hazy	0.135	2.013	1.484	0.626	0.059	0.000	1.093	0.519	0.434	0.000	1.630	0.605
color fading	0.230	1.956	1.752	0.620	−0.24	0.003	1.416	0.506	0.125	0.006	1.719	0.616
artificial light	0.364	2.267	1.419	0.656	0.087	0.009	1.572	0.561	1.508	0.450	1.905	0.635
low-visibility	0.264	0.153	3.994	0.699	0.038	0.004	1.219	0.474	0.151	0.000	3.382	0.597
noise	0.719	0.000	2.240	0.625	0.033	0.001	1.367	0.479	0.800	0.000	2.249	0.589
deep water	0.188	0.424	2.522	0.679	−0.08	0.000	1.261	0.509	0.162	0.045	1.578	0.619
Average	0.436	1.112	2.449	0.647	0.014	0.002	1.329	0.489	**0.554**	0.072	1.968	0.606

its good performance on increasing contrast. However, for all challenging scenes, the values of Q acquired by our method are closer ranging from 0.584 to 0.635.

Additionally, some restored images have a good visual color rendition, but the contrast distortion is often introduced during the image enhancement and restoration process. Therefore, another metric s for quality assessment of contrast namely natural scene statistics (NSS) based quality assessment of contrast-distorted images [58] is provided for contrast quality estimation. The value of s is also positive, and a higher value represents a better outcome. Table 2 shows the evaluation values of s on recovered images of Fig. 6 from all the compared methods. In this Table, the values in bold represent the best results. For indicator s, the results presented in Table 2 show that the obtained values from all compared methods are stable between 2 and 3. However, our approach has the highest mean value with 3.2186, which demonstrate our

Table 2
Quantitative results of s metric of underwater restored images shown in Fig. 6. (The bold values express the best metric values).

Underwater scenes	HE	MSR	DCP [48]	WCID [50]	Li [51]	Ng [53]	Proposed
fuzzy	2.6245	2.4943	2.1021	2.1610	2.6784	**2.7764**	2.4714
hazy	2.6149	3.1069	3.3811	3.1686	3.2250	**3.4479**	3.3423
color fading	2.6240	2.5139	3.4077	3.1830	3.2803	3.4374	**3.4589**
artificial light	2.8562	2.6216	3.3524	3.0624	3.3405	3.4470	**3.3549**
low-visibility	3.1390	2.3557	2.1017	2.4710	**3.4910**	2.1200	3.2553
noise	2.8112	2.6474	2.1894	2.4110	3.1863	2.6703	**3.1876**
deep water	2.7506	3.1896	3.1359	2.9880	3.2309	2.9033	**3.4601**
Average	2.7743	2.7042	2.8100	2.7779	3.2046	2.9718	**3.2186**

Fig. 8. 80 raw tested images taken from several datasets.

Table 3
Average values of five quantitative evaluation metrics for the 150 raw underwater test images, and processing time from all the compared methods. (The bold values express the best metric values).

Method\Metric	e	σ	$\bar{r}$	Q	s	PT (s)
HE	0.272	0.292	**3.025**	**0.623**	2.838	4.775
MSR	0.114	0.001	1.203	0.4323	2.407	**3.371**
DCP [48]	0.246	0.012	1.768	0.562	2.915	9.918
WCID [50]	0.287	**0.000**	2.150	0.542	2.391	11.446
Li [51]	0.302	0.768	2.056	0.608	3.135	10.468
Ng [53]	0.003	0.002	1.304	0.537	2.902	25.428
Proposed	**0.321**	0.010	2.271	0.611	**3.317**	23.985

method stands out among the other six methods in most challenging scenes.

As there is no comprehensive underwater image database for the development of underwater image and video analysis. We extract 150 underwater images from [11,49,59–60], and google images for comparing their results, and then compare the results of different methods on those extracted images. Fig. 8 displays 80 raw underwater test images under different challenging scenes. Table 3 shows the average e, σ, $\bar{r}$, Q and s values for the 150 raw underwater test images from all the compared methods. After more comparative experiments, by observing the statistics in Table 3, we can conclude that our restored algorithm can effectively improve contrast, balance saturation and eliminate nonuniform illumination in terms of e, σ, $\bar{r}$, Q and s values. The higher values of e and s also indicate that our method outperforms the other compared methods in revealing more valuable information (i.e., edge and texture) and increasing contrast. Furthermore, to compare the processing time (PT) of these methods, we selected 20 from the 150 raw underwater test images with the size of 640×480. Their average values of PT are presented in the right column of Table 3. The average PT of the proposed method is 23.985 s. The most time-consuming processing of our algorithm is that it needs multiple iterations. In practice. The cost of one iteration is around 9.6 s, which achieve acceptable outcomes of computational efficiency using the fast ADMM algorithm.

Inspired by [61,62], a subjective experiment is further conducted for perceptual evaluation. We divide the generated total of 1050 images into 150 image sets of 7 images each. The obtained images in the same set are produced by the compared method from the same original image. During the subjective test, a total of 50 image sets from the 150 image sets are randomly selected and assigned to 20 observers. For each image set, the subjects are asked to score the 7 images with a rank from 1 (worst) to 7 (best) based on their own preference. Afterward, the final score called mean opinion score (MOS) is calculated by averaging the 20 subjective scores from all observers. The statistics of the mean values of the MOSs for each method across all tested image sets are illustrated in Fig. 9. In fact, none of these compared methods can create the best restored results for all tested images. However, from Fig. 9, we can observe that our UTV method acquires the highest average score, which indicates that it achieves a superiority in the perceptual evaluation.

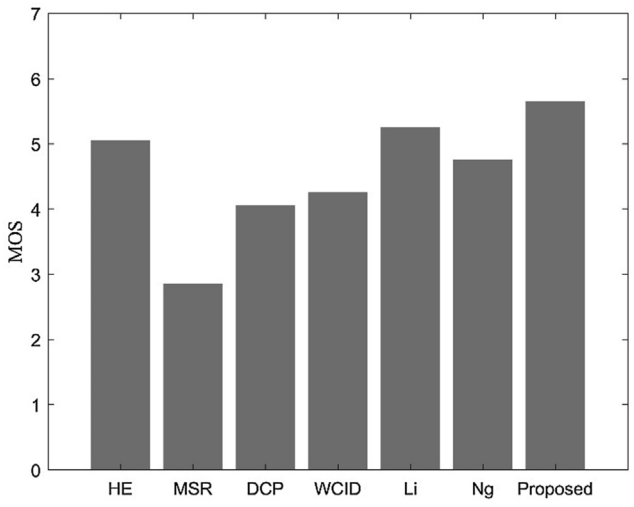

Fig. 9. Mean MOS values of subjective rankings for each method across 50 image sets.

5. Conclusion

In this paper, we establish an underwater variational total model combining underwater dark channel prior. The main contribution of our work is that the underwater image formation model is successfully integrated into the proposed variational model. Moreover, the implementation efficiency of the proposed UTV model is further accelerated by ADMM algorithm. The simultaneous multi-factor variational model and alternating optimization are expected to be effective solutions. A large number of experiments on real-world underwater images present that our restored technique can efficiently improve contrast, reduce noise and remove haze. In addition, in order to validate the superiority of the proposed method, several state-of-the-art underwater image enhancement and restoration methods are employed for comparison. The extensively qualitative and quantitative results and discussions show that the proposed method outperforms these compared algorithms in term of color rendition, non-uniform brightness elimination and edge preservation. The proposed model and algorithm can not only improve the accuracy and speed of underwater image restoration, but also expand their applications in underwater robot operation, oceanographic inspection and other fields such as image understanding and target recognition.

For better combining with subjective evaluation, non-reference metrics are essential to be presented for objective evaluation. In future work, we intend to study the quantitative metrics to evaluate the performance of underwater image enhancement and restoration algorithms. Moreover, we will focus on establishing an underwater image database based on ground truth images for the full-reference image quality objective assessment.

Declaration of Competing Interest

The authors declare that they have no known competing financial interests or personal relationships that could have appeared to influence the work reported in this paper.

Acknowledgment

The research work is partially supported by National Natural Science Foundation of China (No. 61901240), China Scholarship Council (No. 201908370002), the Natural Science Foundation of Shandong Province, China (No. ZR2019BF042, ZR2019MF050), and the China Postdoctoral Science Foundation (No. 2017M612204). The first author also would like to thank Xin Zhao, Xinjie Li, and Jun Xie et al. as the observers for subjective test and Miao Yang for providing the source code of the UCIQE metric.

References

[1] M. Boudhane, B. Nsiri, Underwater image processing method for fish localization and detection in submarine environment, J. Vis. Commun. Image Represent. 39 (2016) 226–238.
[2] M.-C. Chuang, J.-N. Hwang, K. Williams, A feature learning and object recognition framework for underwater fish images, IEEE Trans. Image Process. 25 (4) (Apr. 2016) 1862–1872.
[3] M.-W. Jian et al., The extended marine underwater environment database and baseline evaluations, Appl. Soft Comput. 80 (2019) 425–437.
[4] M.-W. Jian, J.-Y. Qiang Qi, Y.-L Yin Dong, K.-M. Lam, Integrating QDWD with pattern distinctness and local contrast for underwater saliency detection, J. Vis. Commun. Image Represent. 53 (2018) 31–41.
[5] H.-T. Xu, G.-T. Zhai, X.-L. Wu, X.-K. Yang, Generalized equalization model for image enhancement, IEEE Trans. Multimedia 16 (1) (2014) 68–82.
[6] S.-Q. Wang et al., Guided image contrast enhancement based on retrieved images in cloud, IEEE Trans. Multimedia 18 (2) (2016) 219–232.
[7] K. Iqbal, R.A. Salam, A. Osman, A.Z. Talib, Underwater image enhancement using an integrated color model, Int. J. Comput. Sci. 34 (2) (2007) 239–244.
[8] C.-Y. Li, J.-C. Guo, C.-L. Guo, Emerging from water: underwater image color correction based on weakly supervised color transfer, IEEE Signal Process. Lett. 25 (3) (2018) 323–327.
[9] K. Nomura, D. Sugimura, T. Hamamoto, Underwater image color correction using exposure-bracketing imaging, IEEE Signal Process. Lett. 25 (6) (2018) 893–897.
[10] S.G. Narasimhan, S.K. Nayar, Contrast restoration of weather degraded images, IEEE Trans. Pattern Anal. Mach. Intell. 25 (6) (2003) 713–724.
[11] C. Ancuti, C. O. Ancuti, T. Haber, P. Bekaert, Enhancing underwater images and videos by fusion, in: Proc. IEEE Int. Conf. Computer Vision and Pattern Recognition, 2012, pp. 81–88.
[12] C.O. Ancuti, C. Ancuti, C.D. Vleeschouwer, P. Bakaert, Color balance and fusion for underwater image enhancement, IEEE Trans. Image Process. 27 (1) (2018) 379–393.
[13] H.-F. Hu, L. Zhao, X.-B. Li, H. Wang, T.G. Liu, Underwater image recovery under the nonuniform optical field based on polarimetric imaging, IEEE Photonics J. 10 (1) (2018) 6900309.
[14] N. Wang, H.-Y. Zheng, B. Zheng, Underwater image restoration via maximum attenuation identification, IEEE Access 5 (2017) 18941–18952.
[15] N. Wang et al., Two-stage underwater image restoration based on a physical model, Proc. ICGIP 10225 (2016) 2016.
[16] Yi Wang, Hui Liu, Lap-Pui Chau, Single underwater image restoration using adaptive attenuation-curve prior, IEEE Trans. Circuits Syst. I 65 (3) (2018) 992–1002, https://doi.org/10.1109/TCSI.2017.2751671.
[17] M. Zhang, J. Peng, Underwater image restoration based on a new underwater image formation model, IEEE Access 6 (2018) 58634–58644.
[18] C.-Y. Li, J.-C. Guo, Underwater image enhancement by dehazing and color correction, J. Electron. Imaging 24 (3) (2015) 033023.
[19] C.-Y. Li, J.-C. Guo, C.-L. Guo, R.-M. Cong, J.-C. Gong, A hybrid method for underwater image correction, Pattern Recognit. Lett. 94 (15) (2017) 62–67.
[20] S. Bazeille, I. Quidu, L. Jaulin, J.P. Malkasse, Automatic underwater image pre-processing, in: Proc. Caracterisation du Milieu Marin, Brest, France, Oct. 2006, pp. 16–19.
[21] X. Luan et al., Underwater color image enhancement using combining schemes, Mar. Technol. Soc. J. 48 (3) (2014) 57–62.
[22] Huimin Lu, Yujie Li, Xing Xu, Jianru Li, Zhifei Liu, Xin Li, Jianmin Yang, Seiichi Serikawa, Underwater image enhancement method using weighted guided trigonometric filtering and artificial light correction, J. Vis. Commun. Image Represent. 38 (2016) 504–516, https://doi.org/10.1016/j.jvcir.2016.03.029.
[23] P.W. Pan, F. Yuan, E. Cheng, Underwater image de-scattering and enhancing using dehazenet and HWD, J. Mar. Sci. Technol. 26 (4) (2018) 531–540.
[24] W.-Q. Lu, J.-M. Duan, Z.-W. Qiu, Implementation of high-order variational models made easy for image processing, Math. Methods Appl. Sci. 39 (14) (2016) 4208–4233.
[25] J.-M. Duan, Z.-K. Pan, B.-C. Zhang, W.-Q. Liu, X.-C. Tai, Fast algorithm for color texture image inpainting using the non-local CTV model, J. Glob. Optim. 62 (4) (2015) 853–876.
[26] Z. Wang et al., Single image dehazing and denoising combining dark channel prior and variational models, IET Comput. Vision 12 (4) (2018) 393–402.
[27] L. Rudin, S. Osher, E. Fatemi, Nonlinear total variation based noise removal algorithms, Physica D 60 (1–4) (1992) 259–268.
[28] G.-J. Hou, Z.-K. Pan, G.-D. Wang, H. Yang, J.-M. Duan, An efficient nonlocal variational method with application to underwater image restoration, Neurocomputing 369 (2019) 106–121.
[29] L. Tan, W.-Q. Liu, Z.-K. Pan, Color image restoration and inpainting via multi-channel total curvature, Appl. Math. Model. 61 (2018) 280–299.
[30] G.-J. Hou et al., Efficient L-1-based nonlocal total variational model of Retinex for image restoration, J. Electron. Imaging 27 (5) (2018) 051207.
[31] D.-F. Hong, W.-Q. Liu, J. Su, Z.-K. Pan, G.-D. Wang, A novel hierarchical approach for multispectral palmprint recognition, Neurocomputing 151 (2015) 511–521.

[32] D.-F. Hong, W.-F. Liu, X. Wu, Z.-F. Pan, J. Su, Robust palmprint recognition based on the fast variation Vese-Osher model, Neurocomputing 174 (2016) 999–1012.
[33] J.-G. Lu, G.-D. Wang, Z.-K. Pan, Nonlocal active contour model for texture segmentation, Multimedia Tools Appl. 76 (8) (2017) 10991–11001.
[34] Y. Ding et al., Novel Methods for microglia segmentation, feature extraction and classification, IEEE-ACM Trans. Comput. Biol. 14 (6) (2017) 1366–1377.
[35] G.-D. Wang, J.-G. Lu, Z.-K. Pan, Q.-G. Miao, Color texture segmentation based on active contour model with multichannel nonlocal and Tikhonov regularization, Multimedia Tools Appl. 76 (22) (2017) 24515–24526.
[36] G.-J. Hou et al., Image enhancement and restoration: state of the art of variational Retinex models, IAENG Int. J. Comput. Sci. 44 (4) (2017) 445–455.
[37] R. Kimmel, M. Elad, D. Shaked, R. Keshet, I. Sobel, A variational framework for retinex, Int. J. Comput. Vis. 52 (1) (2003) 7–23.
[38] F. Fang, F. Li, T. Zeng, Single image dehazing and denoising: a fast variational approach, SIAM J. Imaging Sci. 7 (2) (2014) 969–996.
[39] J. Liang, X. Zhang, Retinex by higher order total variation L^1 decomposition, J. Math. Imaging Vision 52 (3) (2015) 345–355.
[40] S. Ko et al., Variational framework for low-light image enhancement using optimal transmission map and combined l1 and l2-minimization, Signal Process. Image Commun. 58 (2017) 99–110.
[41] R. Zhang, X.C. Feng, L.X. Yang, L.H. Chang, C. Xu, Global sparse gradient guided variational Retinex model for image enhancement, Signal Process. Image Commun. 58 (2017) 270–281.
[42] Y.-F. Pu et al., A fractional-order variational framework for Retinex: fractional-order partial differential equation-based formulation for multi-scale nonlocal contrast enhancement with texture preserving, IEEE Trans. Image Process. 27 (3) (2018) 1214–1229.
[43] U.A. Nnolim, Analysis of proposed PDE-based underwater image enhancement algorithms, in: Proc. IEEE Int. Conf. Computer Vision and Pattern Recognition, 2016.
[44] U.A. Nnolim, Smoothing and enhancement algorithms for underwater images based on partial differential equations, J. Electron. Imaging 26 (2) (2017) 023009.
[45] B.L. McGlamery, Computer model for underwater camera systems, in: Proc. SPIE 0208, Ocean Optics VI, 1980, pp. 221–231.
[46] J.S. Jaffe, Computer modeling and the design of optimal underwater imaging systems, IEEE J. Ocean. Eng. 15 (2) (1990) 101–111.
[47] Y.-T. Peng, C.C. Pamela, Underwater image restoration based on image blurriness and light absorption, IEEE Trans. Image Process. 26 (4) (2017) 1579–1594.
[48] K. He, J. Sun, X. Tang, Single image haze removal using dark channel prior, IEEE Trans. Knowl. Data Eng. 33 (12) (2011) 2341–2353.
[49] H. Wen, Y. Tian, T. Huang, W. Guo, Single underwater image enhancement with a new optical model, in: Proc. IEEE International Symposium on Circuits and Systems, Beijing, China, May 2013, pp. 753–756.
[50] J.Y. Chiang, Y.C. Chen, Underwater image enhancement by wavelength compensation and dehazing, IEEE Trans. Image Process. 21 (4) (2012) 1–8.
[51] C.-Y. Li, J.-C. Guo, R.-M. Cong, Y.-W. Pang, B. Wang, Underwater image enhancement by dehazing with minimum information loss and histogram distribution prior, IEEE Trans. Image Process. 25 (12) (2016) 5664–5677.
[52] T. Goldstein, B. Donoghue, S. Setzer, R. Baraniuk, Fast alternating direction optimization methods, SIAM J. Imaging Sci. 7 (3) (2014) 1588–1623.
[53] K. Ng Michael, W. Wang, A total variation model for Retinex, SIAM J. Imaging Sci 4 (1) (2011) 345–365.
[54] A. Galdran, D. Pardo, A. Picón, A. Alvarez-Gila, Automatic red-channel underwater image restoration, J. Vis. Commun. Imag. Represent. 26 (2015) 132–145.
[55] N. Hautière, J. Tarel, D. Aubert, E. Dumont, Blind contrast enhancement assessment by gradient ratioing at visible edges, Image Anal. Stereol. 27 (2) (2011) 87–95.
[56] L. Choi, J. You, C. Alan, Referenceless prediction of perceptual fog density and perceptual image defogging, IEEE Trans. Image Process. 24 (11) (2015) 3888–3901.
[57] M. Yang, A. Sowmya, An underwater color image quality evaluation metric, IEEE Trans. Image Process. 24 (12) (2015) 6062–6071.
[58] Y. Fang, K. Ma, Z. Wang, W. Lin, Z. Fang, G. Zhai, No-reference quality assessment of contrast-distorted images based on natural scene Statistics, IEEE Signal Process Lett. 22 (7) (2015) 838–842.
[59] G. Hou et al., Hue preserving-based approach for underwater color image enhancement, IET Image Process. 12 (2) (2018) 292–298.
[60] C.-Y. Li, et al., An underwater image enhancement benchmark dataset and beyond, 2019. https://li-chongyi.github.io/proj_benchmark.html.
[61] K. Ma, W. Liu, W. Zhou, Perceptual evaluation of single image dehazing algorithms, in: Proc. IEEE Int. Conf. Image Process., Quebec, CA, Sep. 2015, pp. 3600–3604.
[62] K. Zeng, Z. Wang, Perceptual evaluation of image denoising algorithms, in: Proc. IEEE Asilomar Conference on Signals, Systems and Computers, Pacific Grove, CA, Nov. 2013, pp. 1351–1355.